LEVERAGE SCORE SAMPLING FOR COMPLETE MODE COVERAGE IN GENERATIVE ADVERSARIAL NETWORKS

A PREPRINT

Joachim Schreurs

Department of Electrical Engineering ESAT-STADIUS, KU Leuven Kasteelpark Arenberg 10, B-3001 Leuven, Belgium joachim.schreurs@kuleuven.be

Hannes De Meulemeester

Department of Electrical Engineering ESAT-STADIUS, KU Leuven Kasteelpark Arenberg 10, B-3001 Leuven, Belgium hannes.demeulemeester@kuleuven.be

Michaël Fanuel*

Univ. Lille, CNRS, Centrale Lille UMR 9189 CRIStAL F-59000 Lille, France michael.fanuel@univ-lille.fr

Bart De Moor

Department of Electrical Engineering ESAT-STADIUS, KU Leuven Kasteelpark Arenberg 10, B-3001 Leuven, Belgium bart.demoor@kuleuven.be

Johan A.K. Suykens

Department of Electrical Engineering ESAT-STADIUS, KU Leuven Kasteelpark Arenberg 10, B-3001 Leuven, Belgium johan.suykens@kuleuven.be

June 6, 2022

ABSTRACT

Commonly, machine learning models minimize an empirical expectation. As a result, the trained models typically perform well for the majority of the data but the performance may deteriorate on less dense regions of the dataset. This issue also arises in generative modeling. A generative model may overlook underrepresented modes that are less frequent in the empirical data distribution. This problem is known as complete mode coverage. We propose a sampling procedure based on ridge leverage scores which significantly improves mode coverage when compared to standard methods and can easily be combined with any GAN. Ridge Leverage Scores (RLSs) are computed by using an explicit feature map, associated with the next-to-last layer of a GAN discriminator or of a pre-trained network, or by using an implicit feature map corresponding to a Gaussian kernel. Multiple evaluations against recent approaches of complete mode coverage show a clear improvement when using the proposed sampling strategy.

1 Introduction

Complete mode coverage is a problem of generative models which has been clearly defined and studied in [1]. In Layman's Terms, a mode is defined as a local maximum of the data probability density. A closely related problem is mode collapse in GANs [2], which happens when a generative model is only capable of generating samples from a subset of all the modes. Multiple GAN variants have been proposed as a solution to this problem, however proposed solutions often assume that every mode has an (almost) equal probability of being sampled, which is often not the case in realistic datasets. Regularly, in critical applications, datasets contain a mixture of different subpopulations where the frequency of each subpopulation can be vastly different. The role of less abundant subpopulations in machine learning

^{*}Most of this work was done when Michaël Fanuel was at KU Leuven.

data has been discussed recently in [3]. Also, it is often common to presume that an algorithm does not have the knowledge of the abundance of subpopulations. It is however important that a machine learning model performs well on all subpopulations. A standard example is medical data where some rare diseases are less abundant than common diseases. To illustrate the approach presented in this paper, a motivating example containing one majority mode and two minority modes is given in Figure 1. When sampling a mini-batch from the Probability Density Function (PDF) p, the side modes can be missed. We observe empirically that this is resolved by sampling from the Ridge Leverage Score (RLS) distribution (see Section 2), which has been extensively used in randomized linear algebra and kernel methods. Figure 1 shows that the samples from the minority modes have larger RLSs. Thus, when sampling from the RLS distribution, there is a higher probability of including the minority modes.

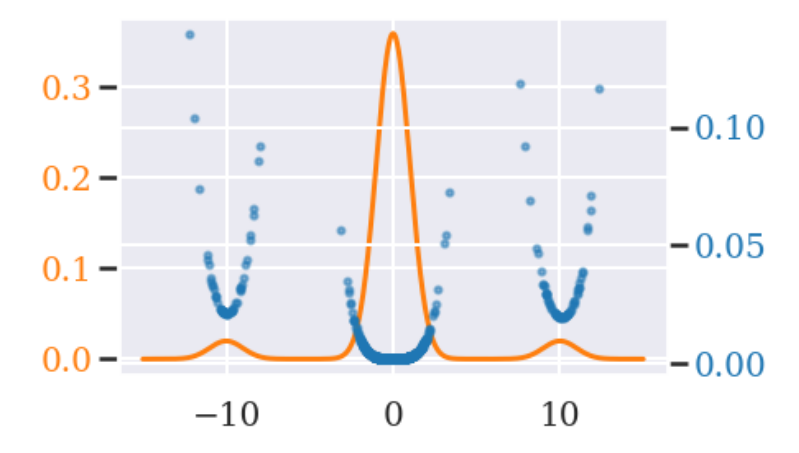


Figure 1: Probability Density Function (orange) and RLS of a sample of this PDF (blue). We take the motivating example from [1], which consists of a 1D target PDF p with 1 majority mode and 2 minority modes: $p=0.9\cdot\mathcal{N}(0,1)+0.05\cdot\mathcal{N}(10,1)+0.05\cdot\mathcal{N}(-10,1)$ given in orange. The RLS distribution is calculated by using a Gaussian kernel with $\sigma=3$ and $\gamma=10^{-3}$. When sampling a mini-batch from the PDF p, the side modes can be missed. This is resolved by sampling from the RLS distribution.

This paper is motivated by two different situations where minority modes can occur:

- the observed empirical distribution is different from the true distribution (biased data), and the data needs to be rebalanced.
- the observed empirical distribution approximates the true distribution sufficiently well, but minority modes consist out of infrequent but very important points, e.g. rare diseases in a medical dataset.

Contribution. When training classical GANs, an empirical expectation of a loss $\mathbb{E}_{x\sim p_d}[\mathcal{L}(x)]$ is optimized in the context of a min-max problem. However, the model often neglects data from minority modes, even though these may be very important. In this work we propose a sampling procedure that promotes sampling out of minority modes by using Ridge Leverage Scores. The common algorithmic procedure simulates the empirical distribution over the dataset $\mathcal{D}=\{x_1,\ldots,x_n\}$ by uniformly sampling over this set. We intentionally bias or distort this process by sampling x_i with probability $p(x_i) \propto \ell_i$, where ℓ_i is the ith ridge leverage score, defined in Section 2. Empirical evidence shows that our procedure rebalances the training distribution, as a result, the GAN model generates samples more uniformly over all modes. RLS sampling can easily be applied to any GAN to improve mode coverage. In particular, using our procedure in combination with a state-of-the-art method for complete mode coverage, a multiplicative weights update procedure given in [1], shows a clear improvement. Finally, RLS sampling is combined with BuresGAN [4] and a state-of-the-art StyleGAN2 with differentiable data augmentations [5], which in both cases consistently improves mode coverage.

Related work. Several works discuss alternative sampling strategies in machine learning. In the context of risk-averse learning, the authors of [6] discuss an adaptive sampling algorithm which performs a stochastic optimization of the Conditional Value-at-Risk (CVaR) of a loss distribution. This strategy promotes models which do not only perform well on average but also on rare data points. In the context of generative models, AdaGAN [7] is a boosting approach to solve the missing mode problem, where at every step a new component is added into a mixture model by running the GAN training algorithm on a re-weighted sample. A similar boosting approach is proposed in [1]. A supervised weighting strategy for GANs is proposed in [8]. In this paper we consider two state-of-the-art GANs that combat mode collapse, PacGAN [9] and BuresGAN [4]. PacGAN uses a procedure called packing. This modifies the discriminator to

make decisions based on multiple samples from the same class, either real or artificially generated. In BuresGAN, an additional diversity metric in the form of the Bures distance between real and fake covariance matrices is added to the generator loss. Note that these methods tackle the traditional mode collapse problem, i.e., the data does not include minority modes. In [10, 11], it was shown that the convergence speed of stochastic gradient descent can be improved by actively selecting mini-batches using DPPs. In [12], coreset-selection is used to create mini-batches with a 'coverage' similar to that of the large batch – in particular the small batch tries to 'cover' all the same modes as are covered in the large batch.

Before proceeding further, we want to discuss two main competitors more in depth.

- The authors of [8] propose a solution to reduce selection bias in training data named Importance Weighted Generative Networks. A rescaling of the empirical data distribution is performed during training. In short, a weighted Maximum Mean Discrepancy (MMD) loss is defined so that the regions where the observed and the target distributions differ are penalized more. If the Radon-Nykodym derivative M between the target and observed distribution is known, each sample $i \in \{1, \ldots, n\}$ is scaled by $1/M(x_i)$. For unknown M, estimation techniques are also provided in [8]. A version of the vanilla GAN (with cross-entropy loss) with importance weighting is introduced (IwGAN), as well as the weighting combined with MMDGAN (IwMmdGAN). In this paper, we will always consider M as known to calculate the weights.
- Another approach to complete mode coverage by [1] and dubbed MwuGAN in this paper, iteratively trains a mixture of generators. At each iteration, the sampling probability is pointwisely normalized so that the probability to sample a missing mode is increased. Hence, this generates a sequence of generative models which constitutes the mixture. More precisely, a weight $w_i > 0$ is given for each $i \in \{1, \dots, n\}$ and initialized such that $w_i = p(x_i)$ for some distribution p_i . Next, a generative model is trained and the probability density $p_i(x_i)$ of each $i \in \{1, \dots, n\}$ is computed. If $p_i(x_i) < \delta p(x_i)$ for some threshold value $\delta \in (0, 1)$, the weight is updated as follows: $w_i \leftarrow 2w_i$, otherwise the weight is not updated. The probability is then recalculated as follows: $p(x_i) = w_i / \sum_j w_j$ for each $i \in \{1, \dots, n\}$. Another generative model is then trained by using $p(x_i)$ and the procedure is repeated.

Classical approach. A GAN consists of a discriminator $D: \mathbb{R}^d \to \mathbb{R}$ and a generator $G: \mathbb{R}^\ell \to \mathbb{R}^d$ which are typically defined by neural networks, and parametrized by real vectors. The value $D(\boldsymbol{x})$ gives the probability that \boldsymbol{x} comes from the empirical distribution, while the generator G maps a point \boldsymbol{z} in the latent space \mathbb{R}^ℓ to a point in input space \mathbb{R}^d . A typical training scheme for a GAN consists in solving, in an alternating way, the following problems:

$$\max_{D} \mathbb{E}_{\mathbf{x} \sim p_d}[\log(D(\mathbf{x}))] + \mathbb{E}_{\tilde{\mathbf{x}} \sim p_g}[\log(1 - D(\tilde{\mathbf{x}}))],$$

$$\min_{G} - \mathbb{E}_{\tilde{\mathbf{x}} \sim p_g}[\log(D(\tilde{\mathbf{x}}))],$$
(1)

which include the vanilla GAN objective associated with the cross-entropy loss. In (1), the first expectation is over the empirical data distribution p_d and the second is over the generated data distribution p_g , implicitly given by the mapping by G of the latent prior distribution $\mathcal{N}(0,\mathbb{I}_\ell)$. The data distribution p_d is typically estimated using the empirical distribution over the training data $\hat{p}_d(\mathbf{x}) = \frac{1}{n} \sum_{\mathbf{x}_i \in \mathcal{D}} \delta\left(\mathbf{x} - \mathbf{x}_i\right)$ as follows: $\mathbb{E}_{p_d(\mathbf{x})}[\mathcal{L}(\mathbf{x})] \approx \mathbb{E}_{\hat{p}_d(\mathbf{x})}[\mathcal{L}(\mathbf{x})] = \frac{1}{n} \sum_{\mathbf{x}_i \in \mathcal{D}} \mathcal{L}\left(\mathbf{x}_i\right)$, where \mathcal{L} is a general loss function. As noted by [13], positive weights w_i for $1 \leq i \leq n$ can be used to construct a weighted empirical distribution $\hat{p}_d^w(\mathbf{x}) = \sum_{\mathbf{x}_i \in \mathcal{D}} w_i \delta\left(\mathbf{x} - \mathbf{x}_i\right)$, then one can apply a weighting strategy to use samples distributed according to $\hat{p}(\mathbf{x})$ to estimate quantities with respect to $\hat{p}_d^w(\mathbf{x})$ as follows:

$$\mathbb{E}_{\hat{p}_{d}^{w}(\mathbf{x})}[\mathcal{L}(\mathbf{x})] = \mathbb{E}_{\hat{p}_{d}(\mathbf{x})} \left[\frac{\hat{p}_{d}^{w}(\mathbf{x})}{\hat{p}_{d}(\mathbf{x})} \mathcal{L}(\mathbf{x}) \right] = \frac{1}{n} \sum_{\mathbf{x}_{i} \in \mathcal{D}} n w_{i} \mathcal{L}(\mathbf{x}_{i}) = \sum_{\mathbf{x}_{i} \in \mathcal{D}} w_{i} \mathcal{L}(\mathbf{x}_{i}).$$
(2)

A stochastic procedure is applied for minimizing the above expectation over \hat{p}_d^w . In this paper, mini-batches are sampled according to the distribution \hat{p}_d^w with w_i given by (3) for $1 \le i \le n$.

2 Sampling with Ridge Leverage Scores

We propose to use a sampling procedure based on the ridge leverage scores [14, 15]. Given a feature map $\varphi(\cdot)$, the corresponding kernel function is $K(x,y) = \varphi(x)^{\top} \varphi(y)$. Let the regularization parameter be $\gamma > 0$. Then, the γ -Ridge

²In [1], this initial distribution is the uniform distribution. We discuss in Section 3.1 a choice of weights based on Ridge Leverage Scores and initialize MwuGAN with the distribution in (3).

Leverage Scores (RLS) are defined for all $1 \le i \le n$ as:

$$\ell_i(\lambda) = \left(K(K + n\gamma \mathbb{I})^{-1}\right)_{ii} = \varphi(x_i)^{\top} (C + n\gamma \mathbb{I})^{-1} \varphi(x_i),$$

where $C = \sum_{i=1}^n \varphi(x_i) \varphi(x_i)^{\top}$ and $K_{ij} = \varphi(x_i)^{\top} \varphi(x_j)$ for $1 \leq i, j \leq n$. Ridge leverage scores are a measure of uniqueness which are used in randomized linear algebra and kernel approximations. They have both a primal and a dual expression that can be leveraged when the size of the feature map or batch-size respectively are too large. When both the batch-size and feature map dimensions are large, one can rely on fast and reliable approximation algorithms with guarantees such as RRLS [16] and BLESS [17]. The role of $\gamma > 0$ is to filter the small eigenvalues of K in the spirit of Tikhonov regularization. RLSs induce the probability distribution

$$p_i = \ell_i / \sum_{j=1}^n \ell_j,\tag{3}$$

for $1 \le i \le n$, which is used classically in randomized methods [14]. Figure 2 illustrates the interpretation of RLSs on two artificial datasets used in this paper. The datasets consist of a mixture of Gaussians. In the RING example, the first 4 modes are minority modes (starting on top and going further clockwise). In the GRID example, the first 10 modes are minority modes (starting left). Similarly to the first illustration (see Figure 1), large RLSs are associated with minority modes. More information on the artifical datasets is given in Section 3.1.



Figure 2: RLS distribution using a Gaussian feature map with $\sigma=0.15$ and regularization $\gamma=10^{-3}$ on the unbalanced RING (left) and GRID (right) data. The darker the shade, the higher the RLS. Dark modes correspond to minority modes.

RLS sampling has a rich history in kernel methods and randomized linear algebra, but has not been used in the context of GANs. One of the key contributions of this paper is to illustrate the use of RLSs in this setting. In order to do so, we propose the use of different feature maps so that RLS sampling can be used both for low dimensional and image data. In what follows, the feature map construction is first discussed. Next, two approximation schemes are introduced.

Choice of feature map. Three choices of feature maps are considered in this paper in order to compute leverage scores:

- Fixed implicit feature map. In low dimensional examples, the feature map φ can be chosen implicitly such that it corresponds to the Gaussian kernel: $\varphi(x)^\top \varphi(y) = \exp\left(-\frac{\|\mathbf{x}-\mathbf{y}\|^2}{\sigma^2}\right)$, where the bandwidth $\sigma>0$ is treated as a hyperparameter. The exact expression of φ is not necessary to calculate RLSs and its definition remains implicit.
- Fixed explicit feature map. For image based data, more advanced similarity metrics are necessary. Therefore, the next-to-last layer of a pre-trained classifier, e.g. the Inception network, is used to extract meaningful features. Note that the classifier does not need to be trained on the exact training dataset, but simply needs to extract meaning full features.
- Discriminator-based explicit feature map. The feature map can be obtained from the next-to-last layer of the discriminator. Let $D(x) = \sigma(w^{\top}\varphi_D(x))$, where $w \in \mathbb{R}^m$ contains the last dense layer's weights and σ is the sigmoid function. This feature map is especially useful in situations where no prior knowledge is available about the dataset.

For a fixed feature map, the RLSs only need to be calculated once for the full dataset before training. The discriminator-based explicit feature map changes throughout the training. Therefore the RLSs need to be recalculated at every step. Nonetheless due to some approximation schemes which are discussed hereafter, the computational cost stays low.

2.1 Approximation schemes

Current day models are highly dimensional, e.g., a DCGAN yields a feature space \mathbb{R}^m of high dimension $m=10^3$. Moreover, the size of datasets is easily a couple of thousand up to a million images. Therefore, two approximation schemes are proposed to speed-up the computation of the ridge leverage scores:

- For the discriminator-based explicit feature map, we propose a two-stage sampling procedure in combination with a Gaussian sketch to reduce the dimension of high dimensional feature maps.
- For the fixed explicit feature map, the well-known UMAP is used to reduce the dimension [18].

Two-stage sampling procedure. For the explicit discriminator based feature map, φ_D has to be re-calculated at each training step. To speed-up the sampling procedure, we propose a sampling procedure in two stages. First, a subset of the data is uniformly sampled, e.g. equal to 20 times the desired batch size. Afterwards, the RLSs are calculated only for the uniformly sampled subset, which are then used to sample the final batch used for training. This two-stage sampling procedure is similar to the core-set selection used in smallGAN [12]. A first difference is that core-sets are selected by combining a Gaussian sketch and a greedy selection in [12], while we use a randomized approach. Second, in this reference, cores-sets are used to reduce the batch size to improve scalability. In contrast, RLS sampling is used here to bias the empirical distribution.

Sketching the discriminator feature map. Gaussian sketching is a commonly used method to reduce data dimension and was also used in [12] and [19] to reduce the dimension of large neural nets. Let S be a sketching matrix of size $m \times k$ such that $S = A/\sqrt{k}$ with A a matrix with i.i.d. zero-mean standard normal entries. Therefore, we consider the following random projection: let a batch be $\{i_1,\ldots,i_m\}\subset\{1,\ldots,n\}$. A random projection of this batch in feature space is then defined as follows:

$$\varphi(x_{i_{\ell}}) = S^{\top} \varphi_D(x_{i_{\ell}}) \in \mathbb{R}^k, \tag{4}$$

for all $\ell \in \{1, \dots, m\}$. This random projection preserves approximately (squared) pairwise distances in the dataset and is motivated by an isometric embedding result in the spirit of Johnson-Linderstauss lemma. Let $0 < \epsilon < 1$ and any integer b > 0. Let k be an integer such that $k \ge 4(\epsilon^2/2 - \epsilon^3/3)^{-1} \log b$. Then, for any set $\{x_1, \dots, x_b\}$ in \mathbb{R}^m there is a map $f: \mathbb{R}^m \to \mathbb{R}^k$ such that for any $\ell, \ell' \in \{1, \dots, b\}$ we have

$$(1 - \epsilon) \|\mathbf{x}_{\ell} - \mathbf{x}_{\ell'}\|_{2}^{2} \le \|f(\mathbf{x}_{\ell}) - f(\mathbf{x}_{\ell'})\|_{2}^{2} \le (1 + \epsilon) \|\mathbf{x}_{\ell} - \mathbf{x}_{\ell'}\|_{2}^{2}.$$

The idea of this work is to consider the set of points given by the batch in the discriminator feature space $x_{\ell} = \varphi_D(x_{i_{\ell}})$ for $1 \leq \ell \leq b$. It is proved in [20] that f exists and can be obtained with high probability with a random projection of the form (4). For a more detailed discussion, we refer to [21].

Dimensionality reduction of the fixed explicit feature map by UMAP. The Gaussian sketch is a simple and fast method to reduce the dimension of the feature map. This makes it a perfect candidate to reduce the dimension of the proposed discriminator feature map, which has to be recalculated at every iteration. Unfortunately this speed comes at a prize, namely the gaussian sketch is deemed too simple to reduce the dimension of highly complex models like the Inception network. Therefore, UMAP is proposed [18]. This non-linear dimensionality reduction technique is able to extract more meaningful features. UMAP is considerably slower than the Gaussian sketch, therefore the use of UMAP is only advised for a fixed feature map like a pre-trained classifier or the Inception network, where the RLSs are only calculated once before training.

3 Numerical experiments

The training procedure is evaluated on a number of synthetic and real datasets, where we artificially introduce some minority modes. The proposed methods are compared with vanilla GAN, PacGAN, MwuGAN, BuresGAN, IwGAN and IwMmdGAN. In particular, MwuGAN outperforms AdAGAN [7] on complete mode coverage problems [1]. Note that PacGAN and BuresGAN are methods to combat mode collapse and not complete mode coverage per se, however they are included for completeness. BuresGAN [4] promotes a matching between the covariance matrices of real and generated data in a feature space defined thanks to the discriminator. Recall that the discriminator is $D(\boldsymbol{x}) = \sigma(w^{\top}\varphi_D(\boldsymbol{x}))$, where w is a weight vector and the sigmoid function is denoted by σ . The normalization $\bar{\varphi}_D(x) = \varphi_D(\boldsymbol{x})/\|\varphi_D(\boldsymbol{x})\|_2$ is used, after the centering of $\varphi_D(\boldsymbol{x})$. Then, the covariance matrix is defined as follows: $C(p) = \mathbb{E}_{\boldsymbol{x} \sim p}[\bar{\varphi}_D(x)\bar{\varphi}_D(x)^{\top}]$. The real data and generated data covariance matrices are denoted by $C_d = C(p_d)$ and

Table 1: Experiments on the synthetic datasets RING and GRID. Sample quality is assessed by counting the number of modes within 3σ of each mode. MwuGAN uses 15 generators. Two RLS BuresGAN are considered. First, RLSs are calculated with an implicit feature map associated with the Gaussian kernel (Gauss.). Second, the next-to-last layer of the discriminator (Discr.) is used to compute the RLSs. RLS MwuGAN is initialized with RLSs using an implicit feature map associated with the Gaussian kernel.

	Ring with	8 modes	Grid with 2	25 modes
	Nb modes (↑)	$\%$ in 3σ (\uparrow)	Nb modes (†)	$\%$ in 3σ (\uparrow)
GAN	-5.0(1.1)	$\overline{0.92(0.02)}$	8.3(3.4)	0.29(0.3)
PacGAN2	5.4(1.4)	0.92 (0.03)	10.3(2.6)	0.13(0.02)
BuresGAN	5.8(1.4)	0.76(0.27)	16.7(0.9)	0.82 (0.01)
RLS GAN Gauss.	7.4(0.9)	0.86(0.05)	13.8(7.4)	0.51(0.32)
RLS GAN Discr.	7.6(0.8)	0.90(0.02)	20.4(2.6)	0.81(0.03)
IwGAN	8(0)	0.85(0.08)	13.4(5.7)	0.29(0.25)
IwMmdGAN	8(0)	0.84(0.02)	1.7(5.1)	0.03(0.05)
MwuGAN (15)	7.9(0.3)	0.86(0.02)	15.2(1.7)	0.47(0.11)
RLS MwuGAN (15) (ours)	8(0)	0.84(0.06)	22.3(1.9)	0.60(0.1)
RLS BuresGAN Gauss. (ours)	8(0)	0.90(0.02)	24.0(1.5)	0.76(0.11)
RLS BuresGAN Discr. (ours)	8(0)	0.90(0.02)	24.4 (0.92)	0.78(0.06)

 $C_g = C(p_g)$, respectively. BuresGAN is described by

$$\max_{D} \mathbb{E}_{\mathbf{x} \sim p_d}[\log(D(\mathbf{x}))] + \mathbb{E}_{\tilde{\mathbf{x}} \sim p_g}[\log(1 - D(\tilde{\mathbf{x}}))]$$

$$\min_{C} - \mathbb{E}_{\tilde{\mathbf{x}} \sim p_g}[\log(D(\tilde{\mathbf{x}}))] + \lambda \mathcal{B}(C_d, C_g)^2,$$
(5)

where the Bures distance $\mathcal{B}\left(C_d,C_g\right)^2=\mathrm{Tr}(C_d+C_g-2\left(C_dC_g\right)^{\frac{1}{2}})$, depends implicitly on $\varphi_D(x)$ (see e.g., [22]).

Overview of proposed methods. The RLS sampling procedure can easily be integrated in any GAN architecture or model. In this spirit, we used RLS sampling with a classical vanilla GAN (RLS GAN) and BuresGAN (RLS BuresGAN). The classical BuresGAN has shown to outperform competitors in mode collapse problems [4]. We noticed empirically that RLS BuresGAN outperformed RLS GAN on the synthetic data (the comparison is shown in Supplementary Material). Therefore we only continue with RLS BuresGAN in the rest of the experiments. Likewise, RLS sampling is combined with MwuGAN, which is considered as state-of-the-art in complete mode coverage. The method, called RLS MwuGAN, uses RLSs as initial starting weights to sample as opposed to uniform weights. Besides the initialization, the method remains unchanged.

Settings. Unless specified otherwise, the models are trained for 30k iterations with a batch size of 64, by using Adam [23] with $\beta_1=0.5,\ \beta_2=0.999$ and learning rate 10^{-3} for both the generator and discriminator. The dimensionality of the generator latent space ℓ is equal to 100. Further information about the used architectures, as well as timings are given in Supplementary Material. The results of this section always refer to the performance achieved at the end of the training. For all the experiments, the reported means and standard deviations are calculated for 10 runs. All the images are scaled in between -1 and 1 before running the algorithms. The hyperparameters of the competing methods are chosen as suggested in the authors' reference implementations. For MwuGAN, we take $\delta=0.25$ and run for an increasing number of generators (displayed in brackets). In all the simulations, PacGAN always uses 2 as packing number. Note that IwMmdGAN and IwGAN require full knowledge of the Radon-Nikodym derivative M, where we want to generate data from a target distribution p but only have access to representative samples from a modified distribution Mp. The method is thus not an unsupervised method, and tackles a slightly different problem. However, the method was included for completeness.

3.1 Synthetic data

Unbalanced versions of two classical synthetic datasets are generated: an unbalanced ring with 4 minority modes (RING) and an unbalanced grid (GRID) with 10 minority modes (see Figure 2). RING is a mixture of eight two-dimensional

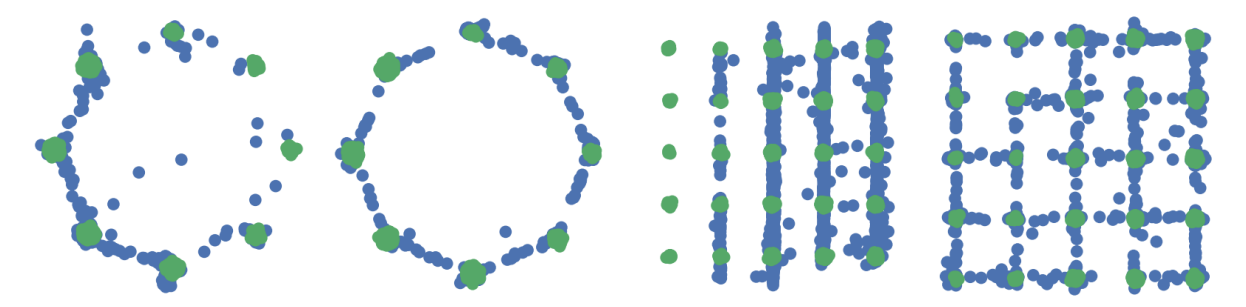


Figure 3: Visualization of the generation quality on RING and GRID. Each column shows 2.5k samples from the trained generator in blue and 2.5k samples from the true distribution in green. The vanilla GAN (first and third) does not cover the minority modes. This is not the case for the RLS BuresGAN Discr. (second and fourth).

isotropic Gaussians in the plane with means $2.5 \times (\cos((2\pi/8)i), \sin((2\pi/8)i))$ and std 0.05 for $i \in \{1, \dots, 8\}$. The probability of sampling from the first 4 consecutive Gaussians is only 0.05 times the probability of sampling from the last 4 modes. GRID is a mixture of 25 two-dimensional isotropic normals with standard deviation 0.05 and with means on a square grid with spacing 2. For one of the first rectangular block of 2×5 adjacent modes, the probability of sampling an individual mode is 0.05 times the probability of sampling an individual mode of the last block of 15 modes.

Evaluation. The evaluation is done by sampling 10k points from the generator network. High-quality samples are within 3 standard deviations of the nearest mode. A mode is covered if there are at least 50 generated samples within 3 standard deviations of the center of the mode. The knowledge of the full Radon-Nikodym derivative M is given to IwMmdGAN and IwGAN by dividing the true probability of each sample (a Gaussian mixture with equal weights) by the adapted Gaussian mixture containing a number of minority modes. The results of the experiments are given in Table 1. For RLS sampling, we use a Gaussian kernel with bandwidth $\sigma=0.15$, and the discriminator network as feature extractor, both with regularization parameter $\gamma=10^{-3}$. The models are trained using a fully connected discriminator and generator architecture using a tanh activation function (see Supplementary Material). As the models are rather simple, no dimensionality reduction is needed.

Generated samples from models trained with and without RLS sampling are displayed in Figure 3. One can clearly see that training a GAN with uniform sampling results in missing the first 4 minority modes. This is solved by using RLS sampling and can be interpreted by comparing the two sampling distributions on Figure 4 (uniform) and Figure 2 (RLS). The RLS are larger for samples in minority modes, which results in a mini-batch that contains samples from all modes. Note that the RLS sampling procedure, given the feature map, is completely unsupervised and has no knowledge of the desired unbiased distribution. The evaluation metrics in Table 1 confirm our suspicions. Only methods designed for complete mode coverage can recover (almost) all modes for the RING dataset. For the unbalanced GRID, only the proposed method has an acceptable performance. Our method even outperforms multiple generator architectures like MwuGAN and RLS MwuGAN, which are considerably more costly to train. Moreover IwGAN, with full knowledge of M, is not capable of consistently capturing all modes. This was pointed out by the authors in [8]: the method may still experience high variance if it rarely sees data points from a class it wants to boost. RLSs can also be used as

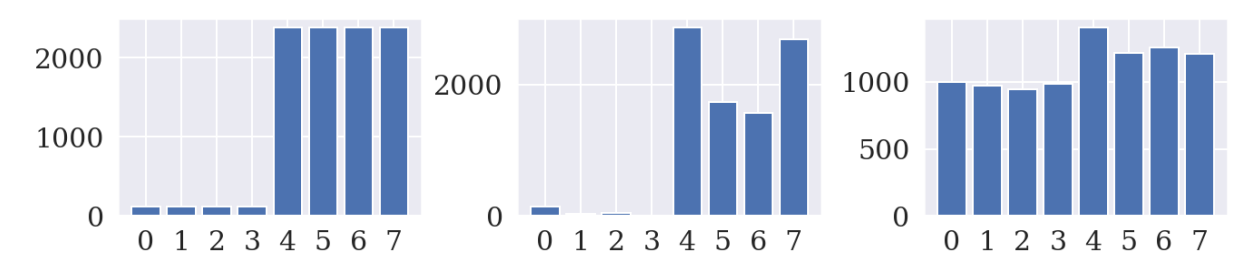


Figure 4: RING. Number of training samples in each mode for the RING dataset (left) Generated samples in each mode by a vanilla GAN (middle). Generated samples by RLS BuresGAN Discr. (right). A rebalancing effect is visible.

initial starting weights in MwuGAN. The RLSs are constructed with a Gaussian kernel with bandwidth $\sigma = 0.15$ and regularization $\gamma = 10^{-3}$. Both the methods contain a mixture of 15 GANs. This approach is compared with the

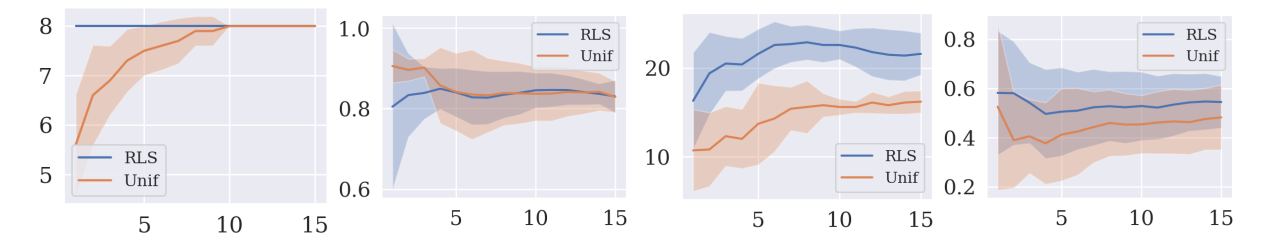


Figure 5: RING: number of modes (top left) and sample quality (top right). GRID: number of modes (bottom left) and sample quality (bottom right). The x-axis refers to the number of generators of MwuGAN. Sample quality is assessed by counting the number of modes within 3σ of each mode. The blue (resp. red) curve indicates the results obtained for RLS (resp. unif.) sampling with MwuGAN.

classical intialization with uniform weights. In Figure 5, a clear improvement over a uniform initialization is visible when RLSs are used to define the initial weights in MwuGAN.

3.2 Unbalanced MNIST

For this experiment, we create two unbalanced datasets out of MNIST. The first modified dataset, named UNBALANCED 012-MNIST, consists of only the digits 0, 1 and 2. The class 2 is then depleted so that the probability of sampling 2 is only 0.05 times the probability of sampling from the digit 0 or 1. This is a similar experiment as in [8], although we increase here the difficulty by making the minority mode even more outspoken. The second dataset, named UNBALANCED MNIST, consists of all digits. The classes 0,1,2,3 and 4 are all depleted so that the probability of sampling out of the minority classes is only 0.05 times the probability of sampling from the majority digits. For these experiments, we use a DCGAN architecture. The exact architecture is given in Supplementary Material. The following metrics are used for performance evaluation: the number of generated digits in each mode, which measures mode collapse, and the KL divergence [24] between the classified labels of the generated samples and a balanced label distribution. The latter measures sample quality. The mode of each generated image is identified by using a standard MNIST classifier which is trained up to 98.43% accuracy on the validation set (see Supplementary Material). The metrics are calculated based on 10k generated images for all the models. For the RLS computation, we use both the discriminator with a Gaussian sketch and the next-to-last layer of the pre-trained classifier with a UMAP dimensionality reduction as feature map. For the UNBALANCED 012-MNIST, both feature maps are reduced to k=25 and the regularization parameter is $\gamma = 10^{-4}$. In the UNBALANCED MNIST, we take k = 10 and $\gamma = 10^{-4}$. An ablation study over different \bar{k} and γ is given in Supplementary Material. We also compare the performance of the classical MwuGAN, initialized with uniform weights, with RLS MwuGAN where the weights are initialized by the RLSs calculated using a the fixed explicit feature map with the same parameters mentioned above. Both the methods contain a mixture of 15 GANs, the experiments are only repeated 3 times for MwuGAN variants.

In our simulations, IwMmdGAN could not be trained succesfully with a DCGAN architecture. The Radon-Nikodym derivative M, which is used by IwMmdGAN and IwGAN, is defined as follows: $M_i=1$ for digits 0 and 1 and $M_i=0.05$ for digits 2, analog for the UNBALANCEDMNIST dataset. Only the proposed models trained with RLS sampling are capable of covering all the modes consistently. The diversity of images generated by RLS BuresGAN can be visualized in Figure 6 where digits from minority modes appear more frequently. A quantitative analysis of mode coverage and sample quality is reported in Tables 2 and 3. In the UNBALANCED 012-MNIST dataset, there is a clear advantage in using RLS sampling with BuresGAN since mode coverage and the KL divergence are improved compared to the other methods. The second best method is RLS MwuGAN which outperforms RLS with uniform starting weights in KL. In the more difficult UNBALANCED MNIST dataset, using the fixed explicit feature map to calculate the RLSs clearly outperforms other methods.

3.3 Unbalanced CIFAR10

We conclude this section with an experiment on colored images, namely the CIFAR10 dataset. This highly diverse dataset contains 32×32 color images from 10 different classes. We consider two unbalanced variations. The first modified dataset, named UNBALANCED 06-CIFAR10, consists of only the classes 0 and 6 or images of airplanes and frogs respectively. The class 0 is then depleted so that the probability of sampling an airplane is only 0.05 times the probability of sampling an image from the class frogs. The second dataset, named UNBALANCED 016-CIFAR10, consists of the classes 0,1 and 6. Compared to the previous dataset, we also add images from the class automobile. Now, the class 6 consisting of frogs is depleted with a factor 0.05. We show the improvement of RLS sampling in

Table 2: Experiments on the UNBALANCED 012-MNIST dataset. Two variants of RLS BuresGAN are trained. First, RLSs are calculated with an explicit feature map obtained from a pre-trained classifier (Class.). The second version uses the next-to-last layer of the discriminator (Discr.) to compute the RLSs. The RLS MwuGAN is initialized using the RLSs with the explicit feature maps obtained from a pre-trained classifier. Minority modes are highlighted in black in the first row.

	Mode 1	Mode 2	Mode 3	KL
GAN	$\overline{4381(172)}$	$\overline{5412(179)}$	129(36)	$\overline{0.31(0.01)}$
PacGAN2	4492(237)	5328(242)	123(29)	0.32(0.01)
BuresGAN	4586(287)	5190(292)	142(19)	0.30(0.01)
IwGAN	4368(295)	5414(287)	147(32)	0.32(0.01)
IwMmdGAN	34(12)	0(0)	69(12)	0.56(0.10)
MwuGAN (15)	4886(473)	4865(466)	176(14)	0.31(0.01)
RLS MwuGAN (15) (ours)	3982(218)	4666(164)	870(65)	0.14(0.01)
RLS BuresGAN Class. (ours)	3414(161)	4862(134)	1461(183)	0.08 (0.01)
RLS BuresGAN Discr. (ours)	5748(172)	2416(268)	1566(293)	0.16(0.02)

Table 3: Experiments on the UNBALANCED MNIST dataset. Two variants of RLS BuresGAN are trained. First, RLSs are calculated with an explicit feature map obtained from a pre-trained classifier (Class.). The second version uses the next-to-last layer of the discriminator (Discr.) to compute the RLSs. The RLS MwuGAN is initialized using the RLSs with the explicit feature maps obtained from a pre-trained classifier. For visualization purposes, we only give the number of samples in the minority modes. The number of samples in the remaining modes is given in Supplementary Material.

	Mode 1	Mode 2	Mode 3	Mode 4	Mode 5	KL
GAN PacGAN2	$\frac{123(22)}{109(29)}$	137(103)	81(31)	161(97)	161(23)	0.48(0.02)
BuresGAN	109(29) $126(31)$	$ \begin{array}{c} 142(70) \\ 157(97) \end{array} $	89(23) $108(30)$	$147(100) \\ 153(62)$	$ 152(40) \\ 147(26) $	$0.48(0.02) \\ 0.46(0.02)$
IwGAN IwMmdGAN	117(33) 1(1)	139(33) 0(0)	97(31) 23(16)	212(69) 1140 (367)	154(34) 3(3)	$0.46(0.02) \\ 1.92(0.1)$
MwuGAN (15) RLS MwuGAN (15) (ours)	144(29) 336(47)	113(28) 283(32)	146(13) 191(23)	172(18) 381(38)	167(28) 276(33)	$0.46(0.02) \\ 0.30(0.02)$
RLS BuresGAN Class. (ours) RLS BuresGAN Discr. (ours)	875 (112) 235(62)	663 (122) 183(141)	360 (198) 264(44)	831(59) 255(109)	615 (82) 219(54)	0.09 (0.01) 0.37(0.02)

a StyleGAN2 with differentiable data augmentation (StyleGAN2 + Aug.) [5]. By a clever use of various types of differentiable augmentations on both real and fake samples, the GAN is able to match the top performance on CIFAR10 with only 20% training data, and is considered state-of-the-art. The StyleGAN2 models are trained for 156k iterations with a mini-batch size of 32 using 'color,translation and cutout' augmentations, which is suggested by the authors when only part of the CIFAR10 dataset is used³. All the other parameters remained the same, only the sampling strategy is changed to RLS sampling in RLS StyleGAN2 + Aug. For the RLS computation, we use the the discriminator feature map with Gaussian sketching and a fixed explicit feature map given by next-to-last layer of the Inception network where UMAP is used to reduce the dimension. For both the RLSs, the dimension is reduced to k=25 and the regularization parameter is set to $\gamma=10^{-4}$. The performance is assessed using 10k generated samples at the end of training by the Inception Score (IS) and the Fréchet inception distance (FID) between the generated fake dataset and the balanced dataset. Mode coverage is evaluated by the number of generated samples in each class. The class of a generated sample is evaluated by a trained CIFAR10 classifier using a resnet56 type architecture [25] which is trained up to 93.77% accuracy⁴. The results of the experiments are given in Table 4, examples of generated images are given in Figure 7. Including RLS sampling in the StyleGAN2 + Aug. clearly improves the performance in unbalanced datasets, this

³The code is taken from https://github.com/mit-han-lab/data-efficient-gans.

⁴The classifier is taken from https://github.com/gahaalt/ResNets-in-tensorflow2.

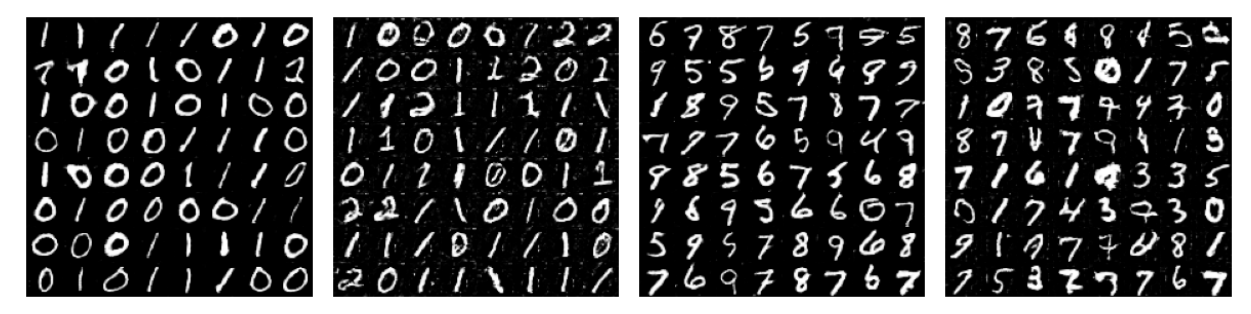


Figure 6: Generated images from UNBALANCED 012-MNIST by a vanilla GAN (first), by RLS BuresGAN Discr. (second) and generated images from UNBALANCED MNIST by a vanilla GAN (third), by RLS BuresGAN Class. (fourth). The minority digits are generated more frequent in the proposed methods that include RLS sampling.

is especially the case for the fixed feature map given by the Inception network. The minority mode is oversampled by approximately a factor 10 or even 100 in the case of the unbalanced 06-CIFAR10 and 016-CIFAR10 datasets respectively. Both the IS and FID also improve significantly. Note that the maximum achievable performance for IS and FID is lower when only a subset of classes is included, as pointed out by [26]. Nonetheless, the relative comparison remains instructive.



Figure 7: Generated images from 06-CIFAR10 by a StyleGAN2 + Aug. (left) and by RLS StyleGAN2 + Aug. (right). Including RLS sampling in the training process promotes sampling from the minority class.

Table 4: Experiments on the UNBALANCED 06-CIFAR10 and UNBALANCED 016-CIFAR10 dataset. Including RLS sampling in the StyleGAN2 + Aug. clearly improves the performance in unbalanced datasets. Minority modes are highlighted in black in the second row.

		06-CIF	AR10			01	6-CIFAR1)	
	Mode 1	Mode 2	IS (†)	FID (↓)	Mode 1	Mode 2	Mode 3	IS (†)	FID (↓)
StyleGAN2 + Aug.	261	9500	4.8	67.5	4526	5206	18	4.3	48.8
RLS StyleGAN2 + Aug. Disc. (ours)	994	8659	5.7	46.4	4449	5132	139	4.6	44.4
RLS StyleGAN2 + Aug. Class. (ours)	2438	7212	6.2	31.3	4156	4393	1155	5.7	27.2

4 Conclusion

We introduced the use of RLS sampling for training GANs. This 'diverse' sampling procedure was motivated by a notion of complete mode coverage in the presence of minority modes. RLS sampling is easy to integrate in any GAN model with only minimal changes to the training procedure. Three feature maps have been discussed. An implicit feature map performs well for low dimensional data. A fixed explicit feature map, such as a pre-trained classifier, achieves good results in high dimensional cases and introduces additional useful information about the data distribution,

obtained from the pre-trained model. Lastly, the discriminator can be used as a feature map when no prior knowledge exists about the data. This allows the sampling to evolve together with the GAN during training. Two approximation methods for the explicit feature maps are also discussed: dimensionality reduction of explicit feature maps and a two-stage sampling procedure to efficiently speed up online RLS computation. We demonstrated empirically that the use of RLS sampling in GANs successfully combats the missing mode problem.

References

- [1] Peilin Zhong, Yuchen Mo, Chang Xiao, Pengyu Chen, and Changxi Zheng. Rethinking generative mode coverage: A pointwise guaranteed approach. In *Advances in Neural Information Processing Systems*, pages 2088–2099, 2019.
- [2] Ian Goodfellow, Jean Pouget-Abadie, Mehdi Mirza, Bing Xu, David Warde-Farley, Sherjil Ozair, Aaron Courville, and Yoshua Bengio. Generative adversarial nets. In *Advances in neural information processing systems*, pages 2672–2680, 2014.
- [3] Vitaly Feldman. Does learning require memorization? a short tale about a long tail. In *Proceedings of the 52nd Annual ACM SIGACT Symposium on Theory of Computing*, STOC 2020, page 954–959, 2020.
- [4] Hannes De Meulemeester, Joachim Schreurs, Michaël Fanuel, Bart De Moor, and Johan AK Suykens. The bures metric for generative adversarial networks. *preprint arXiv:2004.03355*, 2020.
- [5] Shengyu Zhao, Zhijian Liu, Ji Lin, Jun-Yan Zhu, and Song Han. Differentiable augmentation for data-efficient gan training. *preprint arXiv:2006.10738*, 2020.
- [6] Sebastian Curi, Kfir Levy, Stefanie Jegelka, Andreas Krause, et al. Adaptive sampling for stochastic risk-averse learning. accepted at Advances in Neural Information Processing Systems 2020, preprint arXiv:1910.12511, 2019.
- [7] Ilya O Tolstikhin, Sylvain Gelly, Olivier Bousquet, Carl-Johann Simon-Gabriel, and Bernhard Schölkopf. Adagan: Boosting generative models. In *Advances in Neural Information Processing Systems*, pages 5424–5433, 2017.
- [8] Maurice Diesendruck, Ethan R Elenberg, Rajat Sen, Guy W Cole, Sanjay Shakkottai, and Sinead A Williamson. Importance weighted generative networks. In *Joint European Conference on Machine Learning and Knowledge Discovery in Databases*, pages 249–265, 2019.
- [9] Zinan Lin, Ashish Khetan, Giulia Fanti, and Sewoong Oh. Pacgan: The power of two samples in generative adversarial networks. In *Advances in Neural Information Processing Systems*, volume 31, pages 1498–1507, 2018.
- [10] Cheng Zhang, Hedvig Kjellstrom, and Stephan Mandt. Determinantal point processes for mini-batch diversification. *Uncertainty in Artificial Intelligence*, 2017.
- [11] Cheng Zhang, Cengiz Öztireli, Stephan Mandt, and Giampiero Salvi. Active mini-batch sampling using repulsive point processes. In *Proceedings of the AAAI Conference on Artificial Intelligence*, volume 33, pages 5741–5748, 2019.
- [12] Samarth Sinha, Han Zhang, Anirudh Goyal, Yoshua Bengio, Hugo Larochelle, and Augustus Odena. Small-GAN: Speeding up GAN training using core-sets. In *Proceedings of the 37th International Conference on Machine Learning*, volume 119, pages 9005–9015, 2020.
- [13] Austin Tripp, Erik Daxberger, and José Miguel Hernández-Lobato. Sample-efficient optimization in the latent space of deep generative models via weighted retraining. *Advances in Neural Information Processing Systems*, 33, 2020.
- [14] Ahmed Alaoui and Michael W Mahoney. Fast randomized kernel ridge regression with statistical guarantees. In *Neural Information Processing Systems*, pages 775–783, 2015.
- [15] Ping Ma, Michael Mahoney, and Bin Yu. A statistical perspective on algorithmic leveraging. In *Proceedings of the 31st International Conference on Machine Learning*, volume 32 of *Proceedings of Machine Learning Research*, pages 91–99, 2014.
- [16] Cameron Musco and Christopher Musco. Recursive sampling for the nystrom method. In *Advances in Neural Information Processing Systems*, pages 3833–3845, 2017.
- [17] Alessandro Rudi, Daniele Calandriello, Luigi Carratino, and Lorenzo Rosasco. On fast leverage score sampling and optimal learning. In *Advances in Neural Information Processing Systems*, pages 5672–5682, 2018.
- [18] Leland McInnes, John Healy, and James Melville. Umap: Uniform manifold approximation and projection for dimension reduction. *preprint arXiv:1802.03426*, 2018.

- [19] Zichao Yang, Marcin Moczulski, Misha Denil, Nando De Freitas, Alex Smola, Le Song, and Ziyu Wang. Deep fried convnets. In *Proceedings of the IEEE International Conference on Computer Vision*, pages 1476–1483, 2015.
- [20] Sanjoy Dasgupta and Anupam Gupta. An Elementary Proof of a Theorem of Johnson and Lindenstrauss. *Random Struct. Algorithms*, 22(1):60–65, January 2003.
- [21] Samet Oymak, Benjamin Recht, and Mahdi Soltanolkotabi. Isometric sketching of any set via the Restricted Isometry Property. *Information and Inference: A Journal of the IMA*, 7(4):707–726, 03 2018.
- [22] Estelle Massart and P.-A. Absil. Quotient Geometry with Simple Geodesics for the Manifold of Fixed-Rank Positive-Semidefinite Matrices. *SIAM Journal on Matrix Analysis and Applications*, 41(1):171–198, 2020.
- [23] Diederik P Kingma and Jimmy Ba. Adam: A method for stochastic optimization. *International Conference on Learning Representations (ICLR)* 2015, 2014.
- [24] Luke Metz, Ben Poole, David Pfau, and Jascha Sohl-Dickstein. Unrolled Generative Adversarial Networks. In *Proceedings of the International Conference on Learning Representations (ICLR)*, 2017.
- [25] Kaiming He, Xiangyu Zhang, Shaoqing Ren, and Jian Sun. Deep residual learning for image recognition. In *Proceedings of the IEEE conference on computer vision and pattern recognition*, pages 770–778, 2016.
- [26] Mehdi S. M. Sajjadi, Olivier Bachem, Mario Lucic, Olivier Bousquet, and Sylvain Gelly. Assessing generative models via precision and recall. In *Proceedings of the 32nd International Conference on Neural Information Processing Systems*, page 5234–5243, 2018.

A Organization

In Section B, the remaining results from the UNBALANCED MNIST experiment are given. In Section C, the effect of the ridge parameter γ and dimensionality reduction size k is discussed. Then, in Section D, the training times of our simulations are reported. Section E provides further information about the distribution of generated samples in the artificial datasets. Finally, Section F describes the neural network architectures used in the paper.

B Extra table UNBALANCED MNIST dataset

For the UNBALANCED MNIST experiment, only the number of samples in the minority modes are given in the main part. The number of samples for the remaining modes are given in Table 5.

Table 5: Experiments on the UNBALANCED MNIST dataset. Two variants of RLS BuresGAN are trained. First, RLSs are calculated with an explicit feature map obtained from a pre-trained classifier (Class.). The second version uses the next-to-last layer of the discriminator (Discr.) to compute the RLSs. The RLS MwuGAN is initialized using the RLSs with the explicit feature maps obtained from a pre-trained classifier.

	Mode 6	Mode 7	Mode 8	Mode 9	Mode 10
GAN	$\overline{1831(135)}$	1835(32)	2009(69)	$\overline{1747(46)}$	$\overline{1915(143)}$
PacGAN2	1767(116)	1864(16)	1983(105)	1847(25)	1900(110)
BuresGAN	1762(96)	1870(38)	1979(110)	1782(29)	1916(68)
IwGAN	1833(74)	1837(97)	1902(79)	1783(64)	1928(74)
IwMmdGAN	67(45)	0(0)	4(3)	8741(430)	22(10)
MwuGAN (15)	1638(137)	1986(114)	1807(96)	2026(22)	1801(123)
RLS MwuGAN (15) (ours)	1616(17)	1513(144)	2018(78)	1576(30)	1811(34)
RLS BuresGAN Class. (ours) RLS BuresGAN Discr. (ours)	1311(178) 2012(97)	1137(116) 1839(53)	1743(79) 1608(155)	1069(67) 1841(55)	1396(100) 1545(115)

C Effect of the regularization parameter in RLS

C.1 Synthetic data

We display in Table 6 an ablation study for different ridge regularization parameters $\gamma>0$ on the synthetic RING and GRID. A lesson from Table 6 is that the performance on the synthetic datasets does not vary much if different values of γ are chosen in the case of the discriminator feature map. Notice that, for $\gamma=10^{-3}$ and $\gamma=10^{-4}$, there is a small improvement in sample quality for RING and in terms of mode coverage for GRID with the Gaussian kernel feature map.

Table 6: Ablation study over the parameter γ on the synthetic datasets for RLS BuresGAN with a discriminator feature map (Discr.) and Gaussian feature map (Gauss.) with bandwidth $\sigma=0.15$. No significant difference can be seen from the reported performance as the regularization parameter varies.

Feature map	γ	Ring with	n 8 modes	Grid with	25 modes
1 catalo map	/	Nb modes	$\%$ in 3σ	Nb modes	$\%$ in 3σ
Discr.	$ \begin{array}{r} 10^{-2} \\ 10^{-3} \\ 10^{-4} \end{array} $	8(0) 8(0) 8(0)	$ \begin{array}{c} 0.92(0.02) \\ 0.90(0.02) \\ 0.90(0.01) \end{array} $	$ \begin{array}{c} \hline 24.0(1.3) \\ 24.4(0.9) \\ 24.5(0.8) \end{array} $	$ \begin{array}{c} 0.79(0.03) \\ 0.78(0.06) \\ 0.77(0.07) \end{array} $
Gauss.	$ \begin{array}{c} 10^{-2} \\ 10^{-3} \\ 10^{-4} \end{array} $	8(0) 8(0) 8(0)	$0.83(0.10) \\ 0.90(0.02) \\ 0.87(0.04)$	19.9(1.9) 24.0(1.5) 24.8(0.6)	$0.76(0.09) \\ 0.76(0.11) \\ 0.78(0.03)$

C.2 Unbalanced MNIST

We describe here an ablation study for different ridge regularization parameters $\gamma>0$ and size of dimension reduction k on the UNBALANCED 012-MNIST and UNBALANCED MNIST dataset. Moreover, the use of sketching the fixed explicit feature map is analyzed. From these results is concluded that the non-linear UMAP procedure leads to better mode coverage. The results are given in Tables 7 and 8.

D Timings

Training times with a single NVIDIA Tesla P100-SXM2-16GB @1.3 GHz GPU. Temporary evaluations and plotting during training are included in the timings, so only relative comparisons are instructive.

E Distribution of generated samples for the artificial datasets

The number of samples per mode for all GANs in the RING experiments are given in Figure 8. The number of samples per mode for all GANs in the GRID experiments are given in Figure 9.

F Architectures

Table 7: Ablation study over the regularization parameter γ and dimension k on the UNBALANCED 012-MNIST dataset for RLS BuresGAN with a discriminator feature map (Discr.) with sketching and an explicit feature map obtained from the next-to-last layer of a pre-trained classifier (Class.) with a UMAP dimensionality reduction and sketched dimensionality reduction. Minority modes are highlighted in black in the first row. The best performance is achieved using the Discr. sketched and Class. UMAP. feature maps with regularization 10^{-4} and dimension k=25.

Feature map	Dim.	γ	Mode 1	Mode 2	Mode 3	KL
		10^{-2}	$\overline{5561(381)}$	$\overline{2756(300)}$	$\overline{1409(345)}$	$\overline{0.16(0.05)}$
	10	10^{-3}	5568(298)	2769(178)	1386(198)	0.15(0.03)
Discr. Sketched		10^{-4}	5655(279)	2812(135)	1218(253)	0.17(0.04)
		10^{-2}	5814(379)	2405(225)	1501(247)	0.17(0.04)
	25	10^{-3}	5715(312)	2477(139)	1415(310)	0.17(0.04)
		10^{-4}	5748(172)	2416(268)	1566(293)	0.16(0.02)
		10^{-2}	3711(173)	5361(103)	751(161)	0.18(0.03)
	10	10^{-3}	3813(195)	5425(208)	644(67)	0.19(0.01)
Class. UMAP		10^{-4}	3713(221)	5431(226)	712(152)	0.18(0.03)
		10^{-2}	4221(104)	4958(137)	672(109)	0.18(0.02)
	25	10^{-3}	4179(111)	4876(148)	802(105)	0.16(0.01)
		10^{-4}	3414(161)	4862(134)	1461(183)	0.08(0.01)
		10^{-2}	5865(122)	3389(79)	605(111)	0.25(0.03)
	10	10^{-3}	5715(241)	3456(216)	683(161)	0.31(0.01)
Class. Sketched		10^{-4}	5952(309)	3403(206)	513(135)	0.27(0.04)
		10^{-2}	5998(193)	3130(105)	672(119)	0.25(0.03)
	25	10^{-3}	5957(100)	3127(136)	775(95)	0.23(0.01)
		10^{-4}	6009(157)	3138(142)	698(121)	0.32(0.01)

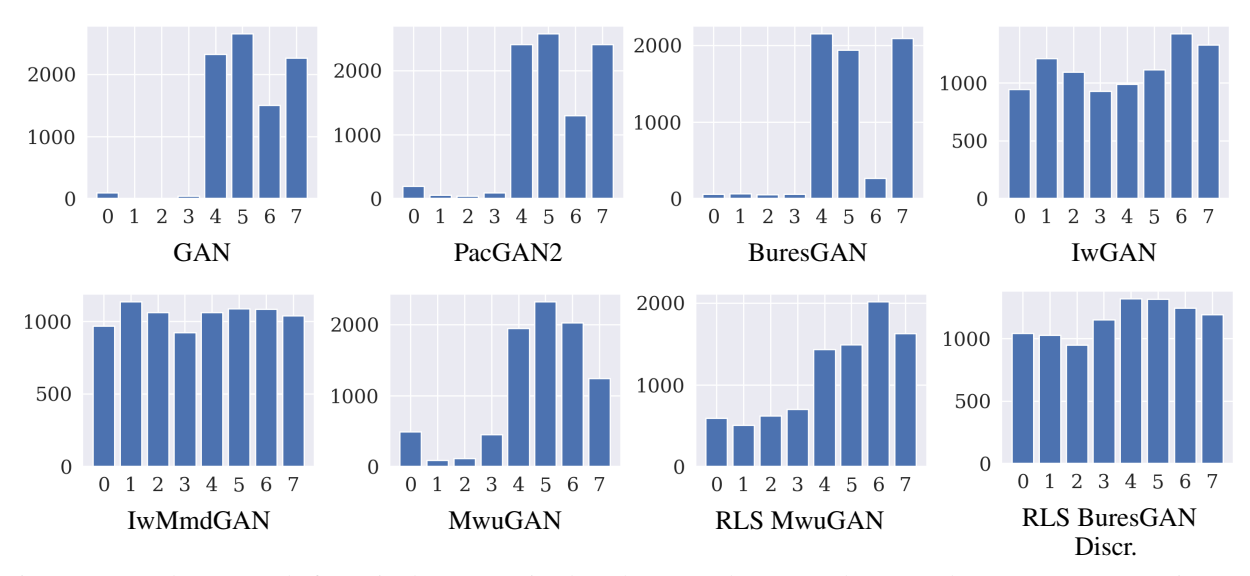


Figure 8: Sampler per mode for a single GAN trained on the RING dataset. Only IwMmdGAN, MwuGAN (15), RLS MwuGAN (15) and RLS BuresGAN with a discriminator feature map (Discr.) are capable of covering all the modes.

Table 8: Ablation study over the regularization parameter γ and dimension k on the UNBALANCED MNIST dataset for RLS BuresGAN with a discriminator feature map (Discr.) with sketching and an explicit feature map obtained from the next-to-last layer of a pre-trained classifier (Class.) with a UMAP dimensionality reduction and sketched dimensionality reduction. Minority modes are highlighted in black in the first row. The best performance is achieved using the Class. UMAP. feature map.

Feature map	Dim.	7	Mode 1	Mode 2	Mode 3	Mode 4	Mode 5	Mode 6	Mode 7	Mode 8	Mode 9	Mode 10	KL
Discr. Sketched	10	$\begin{array}{c} 10^{-2} \\ 10^{-3} \\ 10^{-4} \end{array}$	254(77) 214(38) 235(62)	$\frac{170(30)}{172(123)}$ $183(141)$	222(40) 239(35) 264(44)	227(46) 223(99) 255(109)	$ \begin{array}{c} 212(62) \\ 230(54) \\ 219(54) \end{array} $	2061(94) 2081(91) 2012(97)	1871(134) 1832(32) 1839(53)	$\frac{1598(71)}{1611(100)}$ $1608(155)$	1853(83) 1898(44) 1841(55)	$\frac{1532(96)}{1501(123)}$ $1545(115)$	$\begin{array}{c} 0.38(0.02) \\ 0.39(0.02) \\ 0.37(0.02) \end{array}$
	25	$\begin{array}{c} 10^{-2} \\ 10^{-3} \\ 10^{-4} \end{array}$	236(56) 230(30) 224(49)	191(145) 172(129) 147(179)	286(43) 267(31) 255(27)	231(72) 248(89) 223(52)	219(60) 274(68) 197(53)	2066(113) 2046(100) 2032(116)	$\begin{array}{c} 1765(48) \\ 1780(42) \\ 1790(49) \end{array}$	$\begin{array}{c} 1505(81) \\ 1546(122) \\ 1554(119) \end{array}$	1958(37) 1899(73) 1962(55)	$1543(56) \\ 1538(135) \\ 1617(143)$	$0.37(0.02) \\ 0.37(0.02) \\ 0.40(0.02)$
Class. UMAP	10	$\begin{array}{c} 10^{-2} \\ 10^{-3} \\ 10^{-4} \end{array}$	885(79) 892(137) 875(112)	662(143) 674(90) 663(122)	359(229) 370(227) 360(198)	814(97) 803(108) 831(59)	578(66) 605(75) 615(82)	1248(152) 1187(189) 1311(178)	1137(152) 1123(103) 1137(116)	1847(154) 1784(111) 1743(79)	1095(98) 1110(95) 1069(67)	1374(112) 1452(189) 1396(100)	$\begin{array}{c} 0.10(0.01) \\ 0.09(0.02) \\ 0.09(0.01) \end{array}$
	25	$10^{-2} \\ 10^{-3} \\ 10^{-4}$	556(60) 495(58) 499(73)	$525(82) \\ 473(114) \\ 443(103)$	352(59) $385(50)$ $358(48)$	$542(71) \\ 546(83) \\ 513(104)$	$473(56) \\ 463(50) \\ 450(45)$	$1471(99) \\ 1450(120) \\ 1491(148)$	$1449(87) \\ 1452(69) \\ 1468(51)$	$1915(101) \\ 1964(110) \\ 1957(119)$	$1327(66) \\ 1290(75) \\ 1329(43)$	$ \begin{array}{c} 1392(80) \\ 1483(81) \\ 1493(145) \end{array} $	$0.16(0.01) \\ 0.17(0.02) \\ 0.18(0.01)$
Class. Sketched	10	$ \begin{array}{c} 10^{-2} \\ 10^{-3} \\ 10^{-4} \end{array} $	$ 218(72) \\ 189(45) \\ 239(45) $	188(171) 194(238) 127(200)	165(31) 184(88) 211(27)	261(114) 245(232) 232(133)	246(41) 221(44) 214(65)	2019(166) 2147(176) 2127(113)	1726(48) 1712(38) 1783(48)	1859(204) 1824(182) 1804(122)	1683(63) 1666(61) 1642(29)	1637(178) 1618(177) 1622(142)	$0.38(0.02) \\ 0.4(0.03) \\ 0.48(0.02)$
	25	$\begin{array}{c} 10^{-2} \\ 10^{-3} \\ 10^{-4} \end{array}$	238(30) 262(45) 246(50)	$192(205) \\ 204(116) \\ 220(131)$	$ \begin{array}{c} 189(35) \\ 251(45) \\ 199(41) \end{array} $	308(84) 258(83) 312(70)	254(39) 266(62) 306(41)	$\begin{array}{c} 2011(105) \\ 2041(152) \\ 2033(127) \end{array}$	1699(74) 1621(40) 1689(38)	$\begin{array}{c} 1710(127) \\ 1774(119) \\ 1712(115) \end{array}$	$1785(54) \\ 1751(41) \\ 1724(67)$	$1615(143) \\ 1573(134) \\ 1560(100)$	$\begin{array}{c} 0.36(0.02) \\ 0.35(0.02) \\ 0.34(0.02) \end{array}$

TE 1 1 0 TE : 1			1 10
Table U. Lota	troining	tima in cacande	overeded over III rune
Table 9. Total	i traiiiiii	THE HI SECONDS	, averaged over 10 runs.

	Ring	Grid	012-MNIST	MNIST
GAN PacGAN2	45(1) 65(1)	48(1) 71(1)	$ \begin{array}{c} \hline 1063(4) \\ 1205(4) \\ 1257(2) \end{array} $	$ \begin{array}{c} \hline 1074(3) \\ 1211(8) \\ 1272(2) \end{array} $
BuresGAN IwGAN IwMmdGAN	$ \begin{array}{r} 100(1) \\ \hline 65(1) \\ 45(1) \end{array} $	$ \begin{array}{r} 105(2) \\ \hline 65(1) \\ 56(1) \end{array} $	1357(3) 1066(5) 519(4)	1373(3) 1080(3.3) 5126(1)
MwuGAN (15) RLS MwuGAN (15)	1195(9) 1198(9)	1225(8) 1217(9)	20730(314) 20823(233)	36074(292) 35400(566)
RLS BuresGAN Gauss. RLS BuresGAN Class. RLS BuresGAN Discr.	130(3) / 176(4)	136(2) / 187(1)	/ 1615(11) 2006(3)	/ 2494(8) 2004(2)

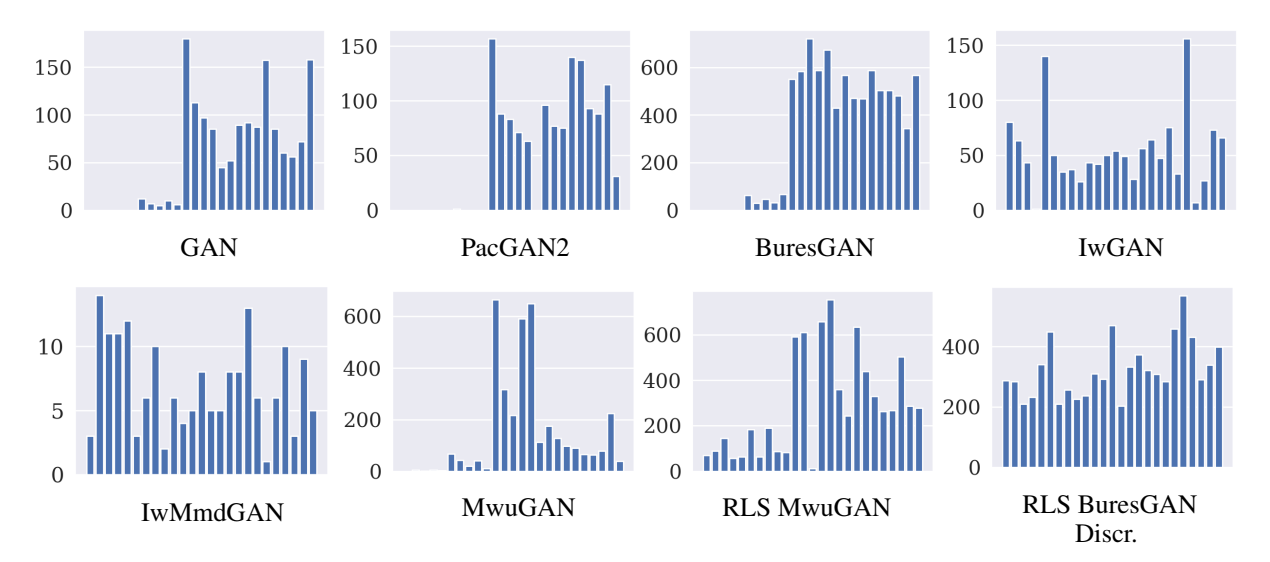


Figure 9: Sampler per mode for a single GAN trained on the GRID dataset. Only the proposed RLS BuresGAN with a discriminator feature map (Discr.) is capable of covering all the modes.

Table 10: The generator (left) and discriminator (right) architectures for the synthetic examples.

Layer	Output	Activation
Input	25	-
Dense	128	tanh
Dense	128	tanh
Dense	2	-

Layer	Output	Activation
Input	2	-
Dense	128	tanh
Dense	128	tanh
Dense	1	-

Table 11: The generator (left) and discriminator (right) architectures for the UNBALANCED 012-MNIST and the UNBALANCED MNIST experiments. BN indicates if batch normalization is used.

Layer	Output	Activation	BN
Input	100	-	-
Dense	12544	ReLU	Yes
Reshape	7, 7, 256	-	-
Conv'	7, 7, 128	ReLU	Yes
Conv'	14, 14, 64	ReLU	Yes
Conv'	28, 28, 1	ReLU	Yes

Layer	Output	Activation	BN
Input	28, 28, 1	-	-
Conv	14, 14, 64	Leaky ReLU	No
Conv	7, 7, 128	Leaky ReLU	Yes
Conv	4, 4, 256	Leaky ReLU	Yes
Conv	2, 2, 512	Leaky ReLU	Yes
Flatten	-	-	-
Dense	1	-	-

Table 12: The CNN architecture of the classifier used during the evaluation of the MNIST experiments. Dropout with a rate of 0.5 is used before the final dense layer.

Layer	Output	Activation
Input	28, 28,1	_
Conv	24, 24, 32	ReLU
MaxPool	12, 12, 32	-
Conv	8, 8, 64	ReLU
MaxPool	4, 4, 64	-
Flatten	-	-
Dense	1024	ReLU
Dense	10	=